Fabrication and Modeling of Dynamic Multipolymer Nanofibrous Scaffolds

Brendon M. Baker
Department of Orthopaedic Surgery, McKay Orthopaedic Research Laboratory, and Department of Bioengineering, University of Pennsylvania, Philadelphia, PA 19104

Nandan L. Nerurkar
Department of Orthopaedic Surgery, McKay Orthopaedic Research Laboratory, University of Pennsylvania, Philadelphia, PA 19104

Jason A. Burdick
Department of Bioengineering, University of Pennsylvania, Philadelphia, PA 19104

Dawn M. Elliott

Robert L. Mauck[1]
Assistant Professor
e-mail: lemauck@mail.med.upenn.edu

Department of Orthopaedic Surgery, McKay Orthopaedic Research Laboratory, and Department of Bioengineering, University of Pennsylvania, Philadelphia, PA 19104

Aligned nanofibrous scaffolds hold tremendous potential for the engineering of dense connective tissues. These biomimetic micropatterns direct organized cell-mediated matrix deposition and can be tuned to possess nonlinear and anisotropic mechanical properties. For these scaffolds to function in vivo, however, they must either recapitulate the full dynamic mechanical range of the native tissue upon implantation or must foster cell infiltration and matrix deposition so as to enable construct maturation to meet these criteria. In our recent studies, we noted that cell infiltration into dense aligned structures is limited but could be expedited via the inclusion of a distinct rapidly eroding sacrificial component. In the present study, we sought to further the fabrication of dynamic nanofibrous constructs by combining multiple-fiber populations, each with distinct mechanical characteristics, into a single composite nanofibrous scaffold. Toward this goal, we developed a novel method for the generation of aligned electrospun composites containing rapidly eroding (PEO), moderately degradable (PLGA and PCL/PLGA), and slowly degrading (PCL) fiber populations. We evaluated the mechanical properties of these composites upon formation and with degradation in a physiologic environment. Furthermore, we employed a hyperelastic constrained-mixture model to capture the nonlinear and time-dependent properties of these scaffolds when formed as single-fiber populations or in multipolymer composites. After validating this model, we demonstrated that by carefully selecting fiber populations with differing mechanical properties and altering the relative fraction of each, a wide range of mechanical properties (and degradation characteristics) can be achieved. This advance allows for the rational design of nanofibrous scaffolds to match native tissue properties and will significantly enhance our ability to fabricate replacements for load-bearing tissues of the musculoskeletal system.
[DOI: 10.1115/1.3192140]

Keywords: electrospinning, fibrous tissue engineering, composite scaffolds, constitutive modeling, temporal properties, mechanical properties

1 Introduction

Fibrous tissues are collagen-rich structures present throughout the musculoskeletal system that serve a variety of vital load-bearing roles. The organization of these tissues is paramount to their mechanical function and is to a great extent dictated by the mechanical environments in which they operate. For example, those tissues that function under cyclic near-uniaxial tension (such as flexor tendons) are comprised of collagen fibers organized in a single predominant direction [1]. On the other hand, tissues that function in more complex multi-axial loading environments, such as the knee meniscus [2–4] and the annulus fibrosus of the intervertebral disk, reveal more complex hierarchical collagen organization [5]. Despite the refined characteristics that function has imparted on the form of these tissues, traumatic injury and degeneration are common occurrences and can interrupt normal mechanical function. As a result, there remains unmet clinical need for engineered replacements for damaged or diseased native fibrous tissues.

When engineering fibrous tissue replacements, the demanding physical environment in which they will perform must be taken into consideration. Tissue engineered constructs should at minimum recapitulate the subfailure stress-strain response of the tissue [6]. Because success in such endeavors has been limited to date, the most common clinical solution for fibrous tissue damage remains the autologous or allogeneic transfer of tissue to the defect site (for example, meniscus transplantation and bone-patella-bone autografts). However, low availability of suitable grafting tissues and high failure rates engender a need for tissue engineered solutions. To specifically address the hierarchical and structural organization of fibrous tissues, many tissue engineering strategies have focused on collagen gel-based constructs. Organization in such constructs is mediated by the traction forces that cells within the collagen gel exert against a fixed boundary and can promote pronounced anisotropy in the forming construct [7,8]. However, these collagen gel-based constructs remain very soft, even after long culture durations, in comparison to native fibrous tissue [9,10]. In other work, hierarchical structure has been imparted through the use of macroscale polymer fibers (including biodegradable polyesters and silk) to engineer fiber-reinforced constructs [11–13]. These scaffolds better recapitulate the native tissue mechanical response and have moved toward clinical implementation.

An alternative strategy that has recently become more prevalent for engineering such tissues is based on the process of electrospinning [14]. This is an old technology, first patented in the 1930s [15], and has been extensively investigated for applications such as textile and filter manufacturing [16]. Within the past decade, this process has found renewed interest for the engineering of a number of different tissues. Compared to macrofibrous construction methods, electrospinning generates nano- and micron-scale fibers, thereby providing a ready means to recapitulate the organizational features and length scales of many collagenous tissues

[1]Corresponding author.
Contributed by the Bioengineering Division of ASME for publication in the JOURNAL OF BIOMECHANICAL ENGINEERING. Manuscript received November 15, 2008; final manuscript received June 2, 2009; published online September 14, 2009. Review conducted by Michael Sacks.

[17]. In its most basic form, electrospinning involves the application of a high voltage potential and resulting gradient to draw a polymer solution into thin fibers, which can then be collected en masse. Numerous processing variables can be varied to fine-tune the electrospinning process, and both biologic and synthetic polymers can be processed in this fashion [18,19]. Moreover, multiple polymers can be combined in the same fiber (intrafibrillar) [18,20], or separate jets can be used to deliver multiple polymers to the same collecting surface [21–23] to modulate the as-formed mechanical properties.

More recently, numerous groups have begun to examine the role of fiber alignment in nanofibrous scaffolds and its potential application for fiber-reinforced tissue engineering. Aligned fibers can be formed by simply focusing deposition onto a rapidly moving surface [24]. We and others have shown that these aligned arrays mimic the structure of numerous fiber-reinforced and anisotropic tissues [17,25–28]. In our previous studies, we used electrospun scaffolds composed of poly(ε-caprolactone) (PCL) and demonstrated that multiple cell types adhere to and organize themselves into aligned communities when cultured on aligned scaffolds. Importantly, with time in culture, the organization of the cell-generated extracellular matrix (ECM) paralleled the governing fiber direction defined by the nanofibrous array [28]. However, we also observed a significant limitation in these scaffolds; surface-seeded cells have difficulty infiltrating through the small pore sizes that result from the dense packing of aligned fibers. This slow infiltration rate results in inhomogeneous ECM deposition and incomplete cell colonization even in relatively thin scaffolds ($\sim$1 mm thick) and over long culture durations ($>$10 weeks).

To address this issue, we developed a dual-polymer electrospinning process that enables the interspersion of a sacrificial fiber population within a dual-component nanofibrous scaffold [23]. These sacrificial fibers, comprised of water-soluble poly(ethyleneoxide) (PEO), serve as space holders during the formation of the scaffold, and their subsequent removal provides the necessary increase in pore size to accelerate cellular ingress. Unfortunately, while the removal of a sufficient fraction of sacrificial fibers enhanced infiltration, it also resulted in an overall loss in scaffold structural integrity as cell-mediated traction forces compacted the construct. Thus, to maintain scaffold integrity while still implementing pore-forming sacrificial fibers, the present work focuses on the inclusion of a more slowly eroding third fiber population. This fiber population would serve to maintain scaffold integrity initially and then gradually erode to augment pore size and porosity as the composite evolves. Inclusion of this third fiber population would provide time-dependent characteristics in the composite scaffold and could also be used to further refine the mechanical properties.

In addition to experimental characterization of scaffold mechanics and porosity as described above, constitutive modeling of these structures can also provide additional insight by permitting investigations that, experimentally, may be laborious or even impossible. Constitutive models of electrospun scaffolds have varied widely in their complexity, from simple geometrically motivated linear models [17,27,29] to hyperelastic continuum models [26,30,31]. Hyperelastic models have the additional advantage of describing materials with nonlinear mechanical behaviors over large deformations. Because nonlinearity and finite deformations are functional hallmarks of many fiber-reinforced soft tissues, hyperelastic models are of great utility not only for characterizing acellular scaffolds and engineered constructs but also for yielding comparisons of these materials with native tissue benchmarks [27,31]. In previous work, we used a fiber-reinforced hyperelastic model to characterize the mechanics of acellular electrospun scaffolds with a single population of PCL nanofibers and used this model to quantify the functional evolution of cell-seeded scaffolds over 8 weeks as ECM was deposited and the constructs matured *in vitro*. The model was validated as a predictive tool for that system and is expanded in the present work to account for the combined behavior of multiple constituent fiber populations.

Table 1 Scaffold fabrication. Polymer formulations used to fabricate composite nanofibrous constructs in Studies I and II.

	Study I		Study II	
	Polymers	Solvent	Polymers	Solvent
Slow	PCL	DMF:THF	PCL	DMF:THF
Medium	PLGA	DMF:THF	PCL/PLGA	DMF:THF
Fast	PEO	90% ethanol	PEO	90% ethanol
Testing	Dry (as-formed)		Wet (time course)	

To carry out this study, we designed and fabricated a novel multijet electrospinning device for the production of aligned composite nanofibrous scaffolds with multiple and distinct fiber populations. Using this device, we formed a composite scaffold containing slow, medium, and fast-eroding elements, and evaluated its mechanical properties (as well as those of its constituent fiber populations). To better understand the mechanical response of these novel composites, we used a hyperelastic model to assess the full nonlinear and anisotropic response of these meshes and developed numerical descriptions of how these properties change over the time course of component degradation. We utilized data from scaffolds containing a single-fiber population, coupled with a constrained-mixture approach, to predict the time-dependent nonlinear tensile behavior of the evolving composite. Finally, we used this validated model to predict the mechanical response of any combination of fiber populations. This new fabrication method and modeling approach provides a means by which rational and directed design can be used to manufacture tissue-specific nanofibrous scaffolds for the engineering of dense connective tissues.

2 Materials and Methods

Two separate studies were performed: Study I included device and methodology development to enable fabrication and testing of multicomponent scaffolds; Study II analyzed and modeled dynamic multicomponent scaffolds over a 9 week time course.

2.1 Scaffold Fabrication. In Study I, solutions of PCL, PLGA, and PEO were electrospun either individually or simultaneously to generate scaffolds with a single-fiber population or with multiple-fiber populations (composite), respectively. All polymers were dissolved by stirring over 18 h at 40°C. PEO (10% w/v, 200kDa, Polysciences, Warrington, PA) was prepared in 90% ethanol, while PLGA (50:50 lactic acid:glycolic acid, 22.2% w/v, 100 kDa, Durect, Pelham, AL) and PCL (14.3% w/v, 80kDa, Sigma, St. Louis, MO) were each dissolved in equal parts dimethylformamide and tetrahydrofuran (DMF:THF, Sigma). Due to the undesirable mechanical characteristics of electrospun PLGA (see Sec. 4), the PLGA solution was replaced with a mixture of PCL and PLGA (termed blend) in Study II. In Study II, PCL and PEO solutions were prepared as described above, and PCL (7.2% w/v) and PLGA (11.1% w/v) were dissolved together in DMF:THF to produce the blended polymer solution (Table 1).

Electrospinning was performed using a custom device designed to focus three electrospun polymer jets from separate spinnerets toward a common centralized rotating mandrel (Fig. 1). Each solution was driven through the spinnerets via syringe pump (KDS100, KD Scientific, Holliston, MA) at 1 ml/h (Study I) or 2.5 ml/h (Study II) from an 18G needle that was translated (with custom fanning devices) over a 5 cm distance along the vertical mandrel (which rotated at a linear surface velocity of $\sim$10 m/s). All three spinnerets were charged to +13 kV and placed 15 cm from the mandrel surface, which was itself charged to -2 kV to enhance fiber collection. Additionally, aluminum plates were positioned at the vertices of this setup and charged to either +9 kV (Study I) or +8 kV (Study II) to focus the electrospun cloud so as

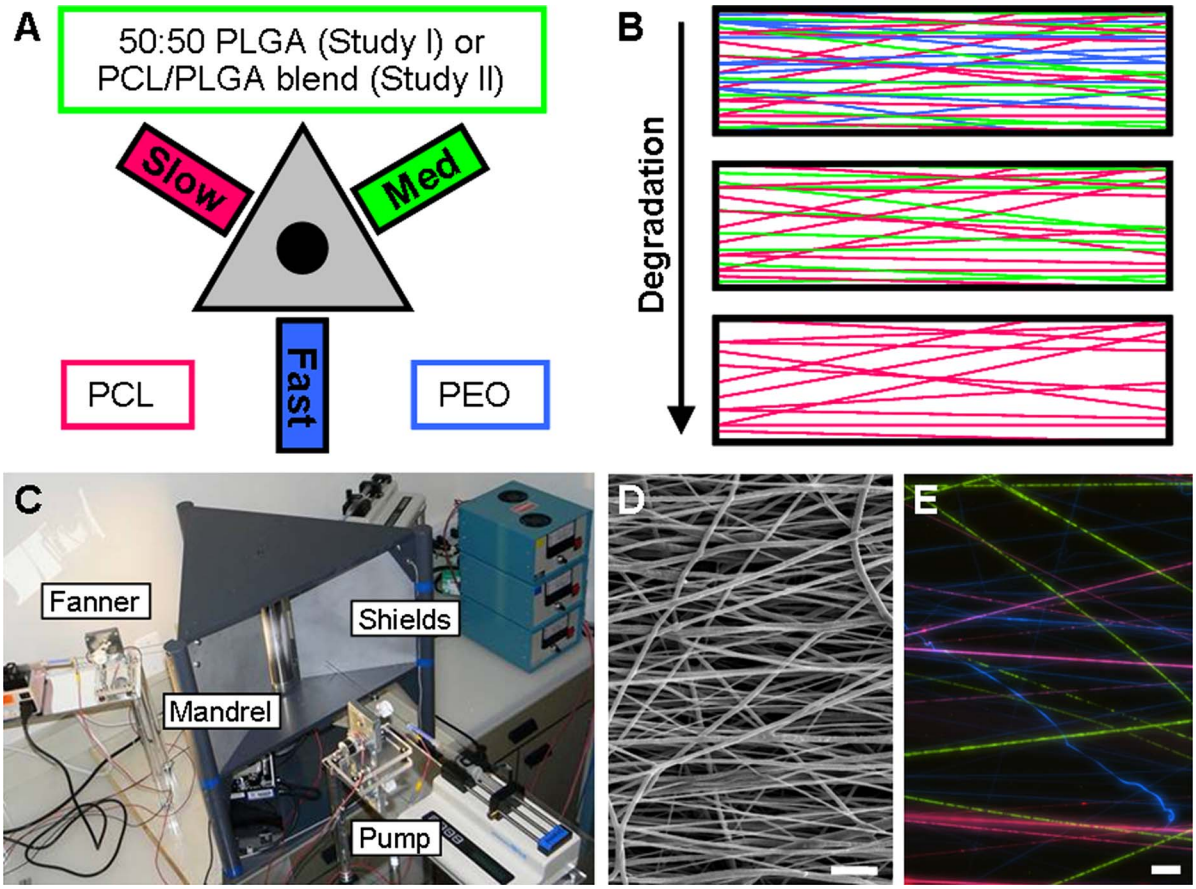

Fig. 1 Composite nanofibrous scaffolds containing three distinct fiber populations were fabricated with a custom electrospinning device. (*a*) Schematic of the formation of electrospun scaffolds containing fast, medium, and slow-degrading fiber populations. (*b*) Diagram depicting the temporal evolution of porosity in composite scaffolds that lose fiber elements in a preprogramed fashion via differing degradation profiles. (*c*) Novel electrospinning device for forming single- and multipolymer fibrous scaffolds by co-electrospinning from up to three jets onto a common rotating mandrel. (*d*) Fiber morphology in composites imaged via SEM (scale bar: 10 μm). (*e*) Composites fabricated with fluorescently labeled fiber populations show the presence and interspersion of each element (scale bar: 10 μm).

to further aid in efficient fiber capture. In both studies, each polymer solution was electrospun individually to generate a mesh containing a single-fiber population; then, all three polymers were co-electrospun onto the same mandrel simultaneously to generate multifiber composites.

2.2 Imaging. In additional studies, polymer solutions were fluorescently doped and electrospun to confirm the presence and interspersion of the three distinct fiber populations. Cell Tracker Red, 7-dimethylaminocoumarin-4-acetic acid (Invitrogen, Carlsbad, CA) and fluorescein (Sigma) were added at 0.2% w/v to solutions of PCL, PEO, and blended PCL/PLGA, respectively. Fluorescently labeled solutions were then co-electrospun for 15 s onto glass cover slips affixed to the rotating mandrel. Fibers were imaged at 20× magnification using a Nikon T30 inverted fluorescent microscope equipped with a charge-coupled device camera and the NIS ELEMENTS software (Nikon Instruments, Inc., Melville, NY). Additionally, PCL, blend, and composite scaffolds were examined by scanning electron microscopy at each time point. Samples were AuPd sputter coated and imaged with a Jeol 6400 scanning electron microscope operating at an accelerating voltage of 10 kV (Penn School of Medicine Microscopy Core Center).

2.3 Mechanical Testing. From each mat, 30×5 mm^2 strips were excised in the prevailing fiber direction (fiber) or perpendicular to this direction (transverse). For Study 1, all testing was performed on as-formed, dry samples. In Study 2, acellular scaffolds were rehydrated and maintained in a standard culture environment (37°C, 5% CO_2) for 9 weeks in order to measure degradation-dependent behavior. After determining the initial dry mass, samples were UV sterilized, rehydrated in diminishing fractions of ethanol (100%, 70%, 50%, 30%), and incubated in DMEM containing 1x PSF at 37°C until testing. For samples from both studies, four measurements of the cross-sectional area were acquired with a custom linear variable transducer/laser system. The strips were airbrushed with black enamel to generate texture before mounting in an Instron 5848 Microtester (Instron, Canton, MA). After a nominal preload of 0.1 N, the samples were allowed 1 min to equilibrate. Following this, the strips were extended beyond their yield point at a rate of 0.1% of the gauge length per second. Images of the central third of each specimen were captured at 0.5 Hz for subsequent texture-correlation analysis via VIC2D to determine two-dimensional Lagrangian strain (E) (Correlation Solutions, Columbia, SC). Modulus was determined from the linear region of the stress-strain plot. Linear regressions were performed iteratively over ranges of 0.6% strain and the yield strain was demarcated when the R^2 transitioned below 0.996. This strain range and R^2 threshold were chosen as conservative and reproducible methods for defining the end of the linear portion of the stress-strain curve and were maintained for analysis throughout the entire study. After tensile testing, samples were dried and reweighed to determine mass loss at each time point.

2.4 Determination of Fiber Fractions. Day 0 samples from Study II were enzymatically digested to estimate starting fiber

fractions of composite scaffolds. PCL, blend, and composite scaffolds were digested with 10 U/ml of Pseudomonas sp. lipase (Type XIII, Sigma) in phosphate buffered saline and incubated at 37°C for 48 h with agitation. After lipase-mediated digestion of the PCL component of each scaffold, samples were washed twice in distilled water before being dried and reweighed.

2.5 Constitutive Modeling of Composites. A hyperelastic fiber-reinforced constitutive model was employed to describe the tensile behavior of hydrated composite nanofibrous scaffolds in Study II. We first determined the constitutive laws for scaffolds composed of single-fiber populations of blend or PCL. These were then applied, using a constrained-mixture approach, to predict the time-varying behavior of the two-component composite scaffold (after the removal of PEO). Upon validation, the model was used to simulate time and composition dependent mechanics.

The composite and single-component scaffolds were modeled using the constitutive theory of highly anisotropic solids as described by Spencer [32], in which the strain energy density function is decomposed into the sum of "fiber" and "matrix" functions.

2.5.1 Single Component Constitutive Laws. For each blend and PCL scaffolds, the matrix phase was described as a compressible neo-Hookean material, while the fibers were described with an exponential law [31,33,34]. As detailed in Nerurkar et. al. [27,31], the resulting constitutive law is given by

$$\mathbf{T}^i = I_3^{-1/2}[\mu^i(\mathbf{F}\mathbf{F}^{\mathbf{T}} - I_3^{\beta^i}\mathbf{I}) + 2\gamma^i(I_4-1)e^{\xi^i(I_4-1)^2})\mathbf{F}\mathbf{a}\otimes\mathbf{a}\mathbf{F}^{\mathbf{T}}] \quad (1)$$

where the superscript i=B, C for blend and PCL, respectively; $\mathbf{T}$ is the Cauchy stress tensor, μ^i and $\nu^i=\beta^i/(1+2\beta^i)$ are the two matrix parameters that characterize matrix modulus and material compressibility; γ^i and ξ^i are the fiber parameters representing the fiber modulus and the degree of their stress-strain nonlinearity; $I_3=\det(\mathbf{C})$ is the third invariant of the right Cauchy–Green tensor $\mathbf{C}=\mathbf{F}^{\mathrm{T}}\mathbf{F}$, where $\mathbf{F}$ is the deformation gradient tensor [35]; the scalar I_4 is an invariant defined as $I_4=\mathbf{a}\cdot\mathbf{C}\mathbf{a}$, where $\mathbf{a}$ is a unit vector along the fiber direction [32]. Fiber contributions were restricted to tensile stresses only ($I_4=1$ for $I_4<1$) [36].

Therefore, each single-fiber population scaffold, blend or PCL, was described by four scalar material parameters: μ^i and ν^i to describe the matrix phase, and γ^i and ξ^i to represent the fiber phase. The implementation of this model for single-component electrospun scaffolds was performed as described previously [31]. In brief, a least squares curve fit of the model to the transverse stress-strain data was performed at each time point to yield matrix material parameters, μ^i and ν^i. The average of the resulting values was used to fit the fiber-direction stress-strain curves in order to determine the time-matched values of fiber parameters, γ^i and ξ^i. Accordingly, the four material parameter values were obtained for each component (blend and PCL) at each time point (days 0, 7, 21, 42, and 63).

2.5.2 Composite Constitutive Law. To model the composite scaffold mechanics, it was assumed that the composite properties were determined entirely by the constituent material parameters and the relative amounts of each constituent present, or

$$\mathbf{T}^t = \mathbf{T}^t(\phi^C,\mu^C,\nu^C,\gamma^C,\xi^C,\phi^B,\mu^B,\nu^B,\gamma^B,\xi^B,\mathbf{C})$$

where $\mathbf{T}^t$ is the total stress of the composite and ϕ^i is the mass fraction of each component. Specifically, a constrained-mixture approach was used, whereby each constituent deforms identically, according to the overall deformation of the composite, or in other words $\mathbf{F}=\mathbf{F}^i$ for $i=B,C$. Additionally, the composite stress is the sum of constituent stresses scaled to their current mass fraction:

$$\mathbf{T}^t = \phi^B\mathbf{T}^B + \phi^C\mathbf{T}^C$$

Conventionally, it is required that the sum of mass fractions always be unity. Although this constraint was enforced at day 0, it was relieved at subsequent time points in order to account for the loss of intact, load-bearing fibers with degradation; mass fractions were computed at each time point as the current constituent mass normalized to the initial total mass. At day 0, it was assumed that $\phi^B=\phi^C=0.5$, based on experiments using lipase to remove the PCL component from both blend and composite scaffolds. From days 7–63, mass fractions were approximated by assuming that all mass loss of the composite (measured experimentally) was due to the loss of the blend component, while $\phi^C=0.5$ was maintained for all time points (see Sec. 4). The contention that PCL mass does not degrade significantly over 63 days was supported by the experimental results. The model was then validated by *predicting* the fiber-direction stress-strain behavior of the composite scaffold at each time point using the time-matched material parameters and mass fractions. For each sample, the experimentally measured 2D deformations were inputted into the model and the resulting model-computed stresses were compared with experimentally measured stress. Agreement of the model predicted stress with the corresponding experimental stress was assessed to indicate the suitability of the proposed model as a full quantitative description of the nanofibrous composite scaffold [31].

2.5.3 Model Simulation. Upon validation, the model was used to simulate the time-varying mechanical behavior of composite nanofibrous scaffolds for a range of initial compositions. In order to approximate the time dependence of the material parameters, each parameter was assumed to vary linearly with time and linear regression was utilized. This assumption proved reasonably accurate for all time-varying parameters (see Sec. 4). The moduli of simulated composites were determined by fitting a tenth order polynomial to the model-generated stress-strain curve and evaluating the derivative of the polynomial at $E=0.1$.

2.6 Statistical Analyses. For experimental data, ANOVA with Bonferroni post hoc tests was used to make comparisons between groups. Data are presented as the mean ± standard deviation from a minimum of 5 samples for each condition and time point. The quality of model fits are reported by the R^2 values as well as the Bland–Altman (BA) limits of agreement (bias ± standard deviation), reported in MPa [37].

3 Results

3.1 Experimental. A custom multijet electrospinning device was successfully constructed and employed to generate single-fiber population and multiple-fiber population composite aligned nanofibrous scaffolds (Fig. 1). Fluorescently labeled fibers demonstrated successful interspersion of discrete fibers throughout the composite scaffold. In Study I, PCL, PLGA, and PEO scaffolds were formed and tested in uniaxial tension in the fiber direction. Stress-strain profiles for each single-fiber population scaffold were distinct (Fig. 2(*a*)). PEO and PCL scaffolds had comparable tensile moduli while the modulus of PLGA scaffolds was ~20 times higher (Fig. 2(*b*)). While PCL scaffolds exhibited a significant toe region and yielded at a higher strain ($E=0.100$), both PEO and PLGA scaffolds lacked toe regions and were significantly less extensible, yielding at $E=0.012$ and $E=0.014$, respectively (Fig. 2(*c*)). When all the three polymers were co-electrospun into a composite scaffold, the resulting mesh displayed characteristics of its constituents (Fig. 2(*a*)). Composite scaffolds had a modulus intermediate to PCL and PLGA (Fig. 2(*b*)) and a toe region was observed, although composite scaffolds still yielded at low strains ($E=0.026$) relative to pure PCL scaffolds (Fig. 2(*c*)). Of note, these scaffolds were all taken from the same location on the rotating mandrel. However, when composite strips were excised from different locations along the length of the mandrel, we observed a gradient in the deposition of PCL and PLGA fibers (Fig. 2(*d*)). Where PLGA fibers were dominant, stress-strain profiles revealed a linear behavior with a higher modulus. Conversely, increases in the PCL fiber fraction resulted in a more pronounced

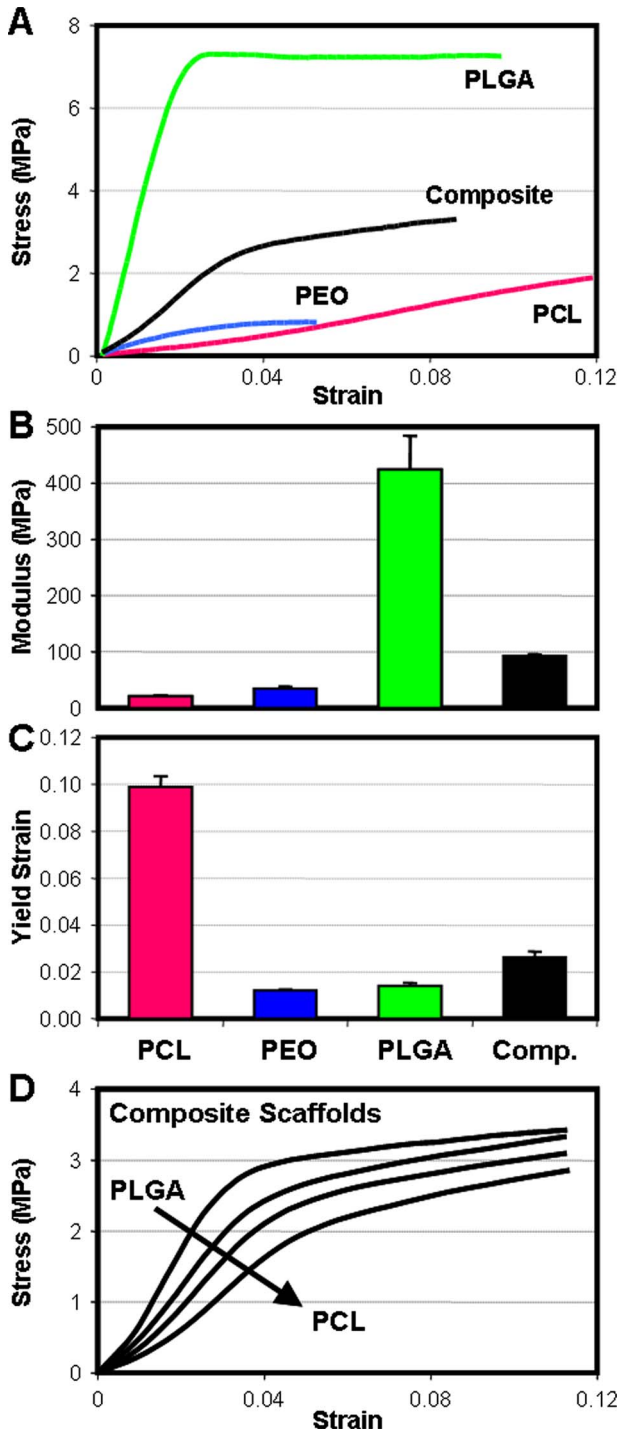

Fig. 2 Study I: Electrospun PCL, PLGA, and PEO scaffolds have unique stress-strain profiles. When all three elements are combined, the composite scaffold stress-strain behavior shares characteristics of each constituent. (*a*) Stress-strain profiles of PCL, PEO, PLGA, and composite scaffolds extended in the fiber direction. Modulus (*b*) and yield strain (*c*) for each scaffold ($n=5$/group). (*d*) Samples from composite scaffolds removed along the length of the mandrel showed a range of behaviors, likely dependent on the relative fractions of PLGA or PCL fibers at each location.

toe region but a lower modulus. This suggests that care must be taken in ensuring full interspersion of composite fibers, particularly when one component has markedly higher mechanical properties than the others. We also noted that, upon hydration, both PLGA and composite scaffolds contracted in length by ~70% and ~60%, respectively (data not shown). Due to this behavior, as well as the low yield strains of PLGA fibers, the PLGA solution was replaced with a blend of PCL and PLGA in Study II.

In Study II, scaffolds comprised of a single-fiber population of blend PCL/PLGA fibers could be hydrated without noticeable decreases in scaffold length or fiber morphology in SEM images (not shown). This allowed for evaluation of scaffold mechanical behavior over a time course of degradation, without the influence of complicating factors such as gross scaffold distortion. For this study, composite scaffolds were hydrated before mechanical analysis. As expected, upon hydration, PEO scaffolds dissolved completely and so are excluded from further analysis of mechanics or mass loss. On day 0 (immediately after hydration), PCL and blend scaffolds tested in the fiber direction demonstrated distinct stress-strain profiles (Fig. 3(*a*)). As in Study I, PCL revealed a significant toe region with yield strains of $E=0.115$ (Fig. 3(*b*)). Blend scaffolds were linear and lacked a toe region but were extensible to higher strains ($E=0.080$) before yield (compared to yield at ~1% for pure PLGA scaffolds evaluated in Study I). Similar to Study I, composites comprised of PCL and blend fibers showed characteristics of the two remaining constituents (recall that PEO is removed upon hydration). Initially, composite scaffolds had moduli intermediate to PCL and blend (Fig. 3(*c*)), but lower strains at yield than both of its constituents (Fig. 3(*b*)). Testing performed on transverse samples revealed the high degree of anisotropy in all three types of scaffolds as evidenced by the significantly lower moduli in the transverse direction (Fig. 3(*d*)).

After the initial day 0 hydration and testing, scaffolds were incubated in DMEM+PSF at 37°C and fiber and transverse properties, as well as changes in mass, were assessed on days 7, 21, 42, and 63. As observed in previous studies, the mass of pure PCL scaffolds did not diminish up to 63 days (Fig. 3(*e*), $p=1.0$). Paralleling the lack of mass loss, the mechanical behavior of PCL scaffolds did not change appreciably, with moduli in both the fiber and transverse directions remaining constant for the entire course of the study (Figs. 3(*c*) and 3(*d*), $p=1.0$). Interestingly, the yield strain of PCL increased with time and was significantly higher than starting values by day 42 (Fig. 3(*b*)). Contrasting the immutability of PCL scaffolds, blend scaffolds began degrading from the outset, as indicated by the significant mass loss by day 7. Additional decreases in mass were observed at all remaining time points, cumulating to an ~40% mass loss by day 63 (Fig. 3(*e*)). Degradation of these blend fibers resulted in decreases in both fiber and transverse moduli in the scaffolds (Figs. 3(*c*) and 3(*d*), $p<0.001$). Additionally, yield strains of blend scaffolds extended in the fiber direction increased with degradation time (Fig. 3(*b*), $p<0.001$).

Composite scaffolds showed time-dependent characteristics as well. These scaffolds lost ~22% of their original mass upon hydration as a result of the immediate dissolution of the PEO fiber population (Fig. 3(*e*)). Lipase digestion after the PEO removal showed that blend fibers made up 54.3% of the remaining composite scaffold, while pure PCL fibers made up 45.7%. Due to the presence of blend fibers, composites continually lost mass for the duration of the study resulting in an additional 18% decrease in mass by day 63. As observed in blend scaffolds, composite scaffolds showed temporal changes in mechanical properties, with both fiber and transverse moduli decreasing in a time-dependent manner (Figs. 3(*c*) and 3(*d*), $p<0.001$). Contrasting blend behavior, the fiber-direction modulus of composites decreased dramatically by day 7 to levels well below PCL and blend values ($p<0.001$), and then appeared to stabilize toward later time points. As with PCL and blend scaffolds, composite yield strains increased with time ($p<0.001$) approaching $E=0.122$ by day 63.

3.2 Theoretical. The constitutive model was successfully fit to transverse PCL and blend constructs at all time points to yield matrix constants μ^i and ν^i (Figs. 4(*b*) and 4(*c*), Table 2), with

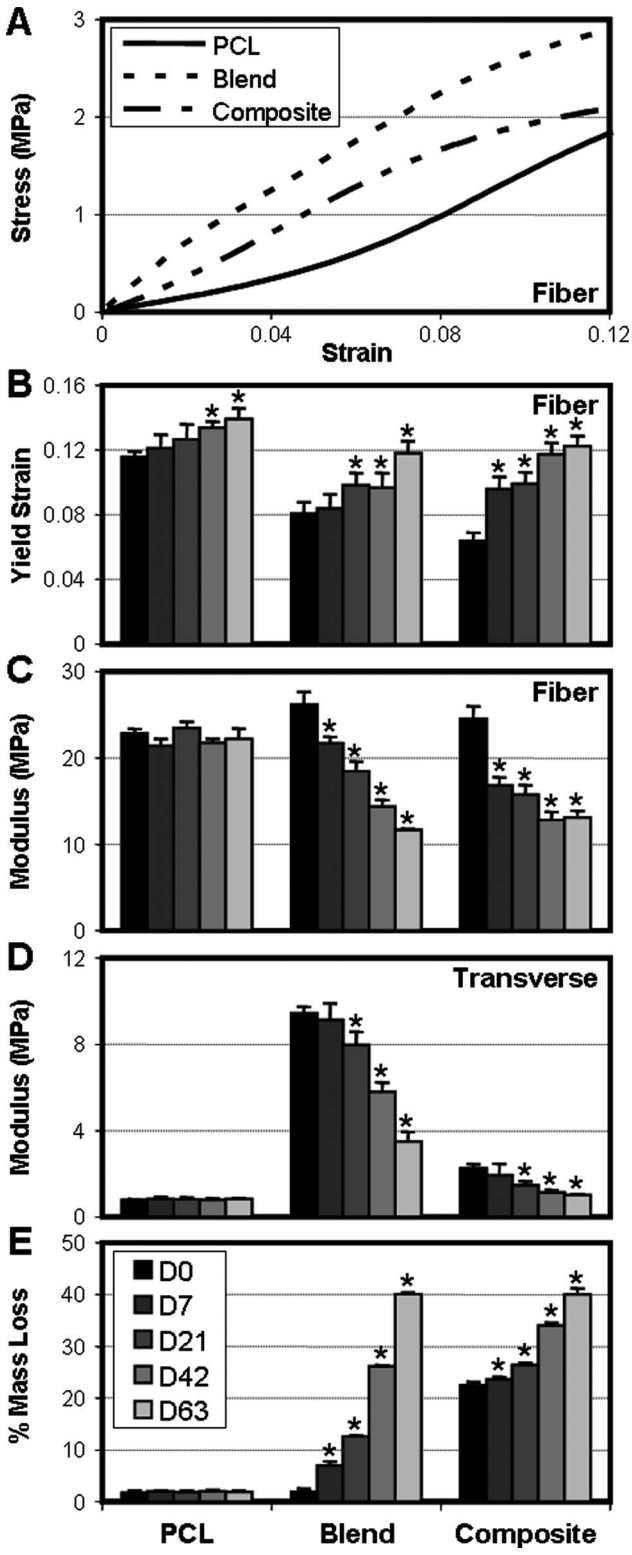

Fig. 3 Study II: Single- and multiple-fiber population scaffold tensile behaviors are modulated by composition and degradation time. (*a*) Stress-strain curves of day 0 PCL, blend, and composite scaffolds tested in the fiber direction. Yield strain (*b*) and modulus (*c*) of samples tested in the fiber direction over 63 days ($n=5$/group per time point). (*d*) Modulus in the transverse direction as a function of time ($n=5$/group per time point). (*e*) Percent mass loss relative to dry, as-formed samples over the 63 day time course ($n=5$/group per time point). Note that composite scaffolds on day 0 lose ~22% of their starting mass due to the removal of the PEO fiber population during hydration. $*: p<0.01$ versus day 0.

average $R^2=0.986$ and BA -0.002 ± 0.004 MPa. As an example, model fits to experimental data of day 0 samples tested in the transverse direction are shown in Fig. 4(*a*). The blend matrix parameter μ^B decreased linearly with time by up to 2.5-fold on day 63. No significant changes were observed in μ^C, ν^C, or ν^B with time. The constitutive model also successfully fit blend and PCL samples along the fiber direction to yield fiber parameters γ^j and ξ^j with average $R^2=0.988$ and BA -0.018 ± 0.055 MPa (Figs. 4(*e*) and 4(*f*)). Model fits to fiber-direction experimental data of day 0 samples are shown in Fig. 4(*d*). The fiber modulus parameter γ^j decreased approximately twofold with time for blend samples but did not change with time for PCL. ξ^C increased slightly by day 63, and ξ^B was zero at all time points.

Having determined the time-varying material parameters for each single-fiber population scaffold, we next used this information to predict the behavior of the composite scaffold. Accurate prediction of the composite scaffold mechanics would indicate that the model is valid for this application. The model was successfully validated at each time point, using only the deformation, the relative amount of blend to PCL fibers remaining, and the material parameters from each time point to *predict* the composite scaffold stress under uniaxial extension in the fiber direction (Fig. 5, average $R^2=0.997$ and BA -0.013 ± 0.053 MPa, Table 2). Although at day 0 the model underpredicted stresses, it provided strikingly close predictions of experimental stress-strain curves at each subsequent time point (Table 2).

Using the validated model, we next predicted the modulus and curvature of theoretical scaffolds consisting of any combination of PCL and blend at any time point. The model simulation indicated that the composite scaffold modulus can be tuned between 20 MPa and 45 MPa by simply varying the initial content of blend or PCL, although some inaccuracy is observed in this estimation due to the dependence of yield strain on composition which the hyperelastic model does not capture. Specifically, moduli were computed at deformations sufficiently large to capture the linear region of high PCL content samples, and all composites were assumed to deform elastically in this same range (Fig. 6(*a*)). Additionally, the simulation revealed that composite mechanics are increasingly sensitive to degradation with time as the blend content is increased. Finally, by varying the balance between blend and PCL fiber populations, the model demonstrated that the magnitude and the nonlinearity of the composite stress-strain behavior can both be modulated (Fig. 6(*b*)).

4 Discussion

Electrospun nanofibrous scaffolds hold great promise for the tissue engineering of fibrous elements of the musculoskeletal system. The electrospinning process is inexpensive, straightforward, and easily modified to produce scaffolds with a range of mechanical and degradation characteristics [18,38]. Furthermore, the alignment of nanometer- to micron-scale fibers engenders structural and mechanical anisotropies in scaffolds comparable to that of many soft tissues [17,27,28,39]. However, the mechanical behavior of native tissues is complex, with most showing not only pronounced anisotropy but also nonlinear stress-strain profiles [40]. Both "toe" and "linear" properties are critical for normal tissue response; toe region properties are essential for flexibility, while linear region properties resist extreme deformations at high loads. These nonlinear properties are dependent on the complex interplay of numerous tissue constituents, including fibers (e.g., collagens), matrix (e.g., proteoglycans and water), and fiber-matrix interactions (e.g., cross-linking molecules) [41,42].

While the target tissues are complex, most electrospinning efforts to date have relied upon the use of a single polymeric fiber population for scaffold formation. The number of polymers that can be electrospun is increasing at a rapid rate and these fibers show a diverse array of mechanical properties, including some with nonlinear behaviors. However, it is somewhat unreasonable to suppose that a single-fiber population can recapitulate the intri-

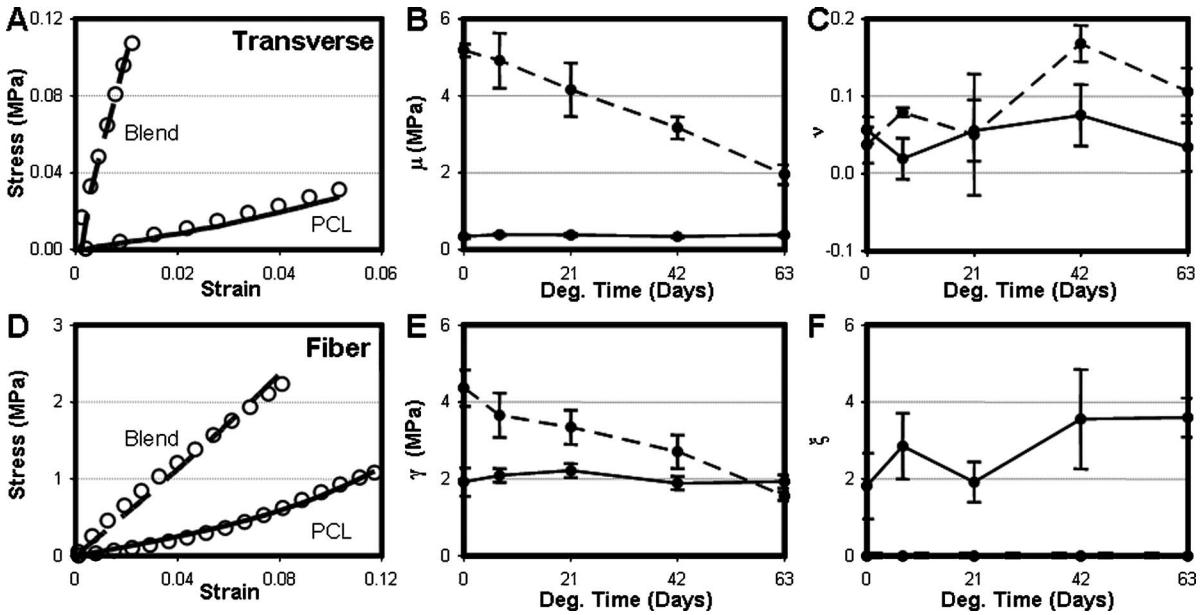

Fig. 4 Characterization of single-fiber population (PCL (solid) and blend (dashed)) scaffold tensile behavior with a hyperelastic fiber-reinforced constitutive model. Curve fit results (lines) on day 0 are shown along with experimental data (circles) for the transverse (*a*) and fiber (*d*) directions. From transverse direction testing, matrix parameters μ (*b*) and ν (*c*) were determined at each time point. These values, coupled with fits to fiber-direction data at each time point, were used to determine fiber parameters, γ (*e*) and ξ (*f*).

cate mechanical behavior of native tissues. This would therefore limit scaffold applications to non-load-bearing situations or rely on cell-mediated ECM deposition to provide tissue-specific functionality. We have shown that, with extended periods of *in vitro* preculture, cells seeded onto aligned scaffold can improve functional properties and impart increasing nonlinearity [31,43]. An ideal scaffold would, however, match the native tissue properties over the entire time course of maturation. We hypothesized that such complex features might be achieved by combining multiple-fiber populations, each with distinct mechanical characteristics, into a single composite nanofibrous scaffold.

The particular polymer set chosen for this work is commercially available, widely applied, and is generally considered to be biocompatible upon implantation. Previous work from our group identified PCL as a suitable electrospun polymer as it is distensible to high strains before yield, exhibits a toe region akin to that of fibrous tissues, and is stable in culture for long durations [38,43]. However, due to the dense packing of nanofibers in aligned PCL scaffolds, pore size is limited and thus cell infiltration and matrix deposition are slow and inhomogeneous [28,31]. To increase porosity of these scaffolds, we developed methods for the incorporation of sacrificial pore-forming fibers [23]. In that study, it was observed that the removal of increasing fractions of sacrificial fibers correlated linearly with decreases in scaffold properties. Since cell infiltration was enhanced only at >50% sacrificial fiber content, a 50% decline in initial scaffold properties would be required to hasten colonization. Furthermore, because dissolution of the sacrificial PEO fibers is "all-or-none," these mechanical changes occur very rapidly, and so cell-mediated contraction can result in distortion of the scaffold shape.

To specifically address this issue, we sought to include a stiffer slower degrading fiber population in these composite structures. Based on previous reports in the literature, PLGA was chosen for its high stiffness and moderate degradation rate. In Study I, PLGA was successfully electrospun and incorporated into composite scaffolds. Single-fiber population PLGA scaffolds were very stiff (~20-fold higher than PCL); however, two significant limitations were observed. First, consistent with previous reports [38], pure PLGA scaffolds could only be deformed by ~1% before succumbing to permanent deformation and/or failure. Thus when PLGA was electrospun into the composite scaffold, the resulting yield strain was reduced by a factor of 4, to $E=0.025$. As most fibrous tissues experience deformations on the order of 5–10%,

Table 2 Model validation. R^2 and Bland–Altman limit of agreements from least squares fits of experimental data for single-fiber population scaffolds (PCL and blend). Also shown are metrics comparing composite scaffold experimental stress-strain response and model predicted values.

	Model Fits								Model predictions	
	PCL				Blend				Composite	
	Fiber		Transverse		Fiber		Transverse		Fiber	
	R^2	BA (MPa)	R^2	BA (MPa)	R^2	BA (MPa)	R^2	BA (MPa)	R^2	BA (MPa)
Day 0	0.987 ± 0.005	0.010 ± 0.044	0.998 ± 0.002	0.000 ± 0.001	0.984 ± 0.004	−0.052 ± 0.104	0.979 ± 0.006	−0.005 ± 0.009	0.997 ± 0.002	−0.151 ± 0.105
Day 7	0.995 ± 0.001	0.005 ± 0.025	0.999 ± 0.080	0.000 ± 0.001	0.967 ± 0.003	−0.053 ± 0.096	0.984 ± 0.003	−0.004 ± 0.008	1.000 ± 0.000	0.028 ± 0.027
Day 21	0.992 ± 0.001	0.006 ± 0.032	0.995 ± 0.006	−0.001 ± 0.002	0.989 ± 0.005	−0.043 ± 0.081	0.977 ± 0.017	−0.004 ± 0.008	0.998 ± 0.001	0.064 ± 0.049
Day 42	0.991 ± 0.004	0.005 ± 0.038	0.996 ± 0.007	0.000 ± 0.002	0.984 ± 0.004	−0.049 ± 0.083	0.965 ± 0.005	−0.004 ± 0.007	0.996 ± 0.001	0.039 ± 0.045
Day 63	0.994 ± 0.001	0.005 ± 0.023	0.995 ± 0.008	0.000 ± 0.001	0.994 ± 0.002	−0.011 ± 0.020	0.974 ± 0.009	−0.002 ± 0.004	0.995 ± 0.001	−0.046 ± 0.041

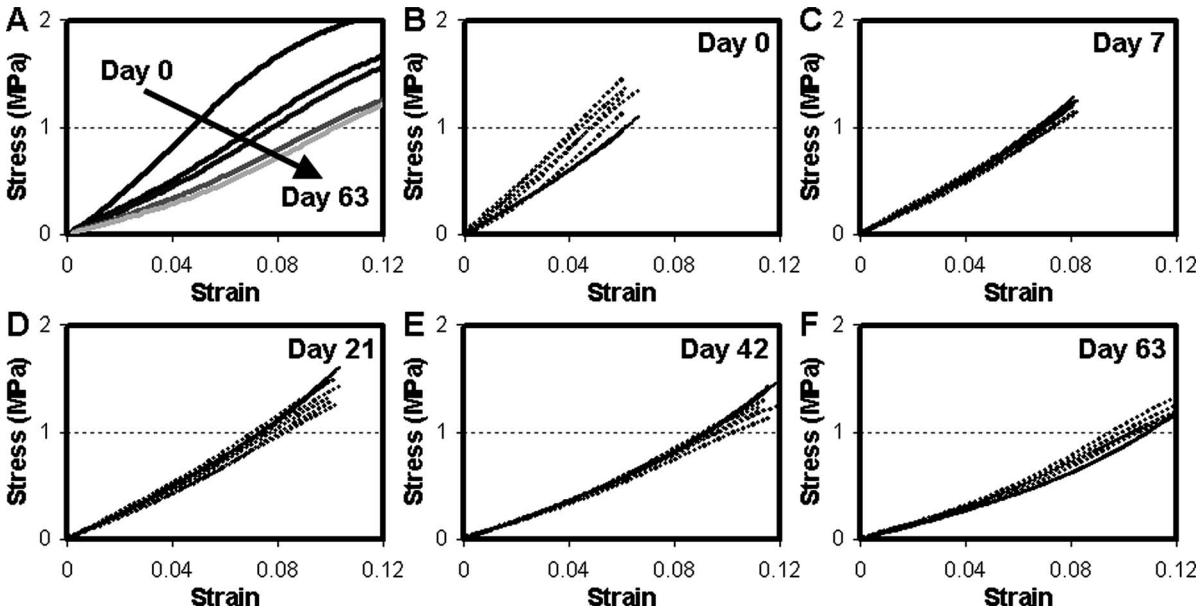

Fig. 5 Material parameters from single-component scaffolds successfully predict composite scaffold behavior. (*a*) Stress-strain curves for composites tested in the fiber direction. Stress-strain profiles diminished as degradation occurred over 63 days, due to the decreasing properties of the blend fiber population. Model predictions of composite stress response when tested in the fiber direction on days 0 (*b*), 7 (*c*), 21 (*d*), 42 (*e*), and 63 (*f*) showed good agreement with experimental measures. Each plot contains all five experimental curves (dotted lines) and the corresponding five model-generated predictions (solid lines).

we considered this attribute to be a serious deterrent to using pure PLGA fibers. Additionally, and through a mechanism not yet fully understood, PLGA scaffolds underwent severe contraction and thickening immediately upon hydration, precluding a longitudinal study of mechanical properties with degradation.

Previous work by Barnes et al. [18] had demonstrated that inelastic polymers (such as PLGA) could be made more elastic with the inclusion of PCL. Thus, in Study II, we utilized a blended solution of PLGA and PCL to introduce temporal characteristics to the composite. The modulus of pure blend scaffolds was significantly lower than that of pure PLGA, although its yield strain (~8%) was markedly higher. These changes are possibly due to alterations in crystallinity within each fiber strand, although this was not assessed in the current study. Blend scaffolds could be hydrated without the gross distortion, as had been observed for pure PLGA fibers. Interestingly, the removal of the PCL component of blend fibers on day 0 (via lipase digestion) caused the remaining PLGA portion to contract, confirming a secondary role of PCL as an intrafibrillar stabilizer (not shown). With this blend component, we evaluated the temporal characteristics of composite scaffolds. Instantaneous removal of PEO from the composite resulted in an ~22% mass loss upon hydration. Conversely, blend fibers (formed into single-component scaffolds) degraded slowly over 9 weeks, with corresponding decreases in mechanical properties. Composite scaffolds containing blend populations showed similar time-dependent decreases in mechanical properties, while pure PCL scaffolds did not change, suggesting that these dynamic characteristics arise from the degrading blend component. The mechanism by which blend scaffolds (or fibers) degrade was not assessed. While the idealized mechanism shown in Fig. 1(*b*) suggests degradation resulting in complete fiber removal, blend fibers may undergo scission and complete removal or may experience internal changes that leave the fiber present but in a weakened state. Scanning electron microscopy (SEM) imaging over the time course did not reveal obvious structural changes, although this may be an inherent limitation of the 2D imaging modality. The

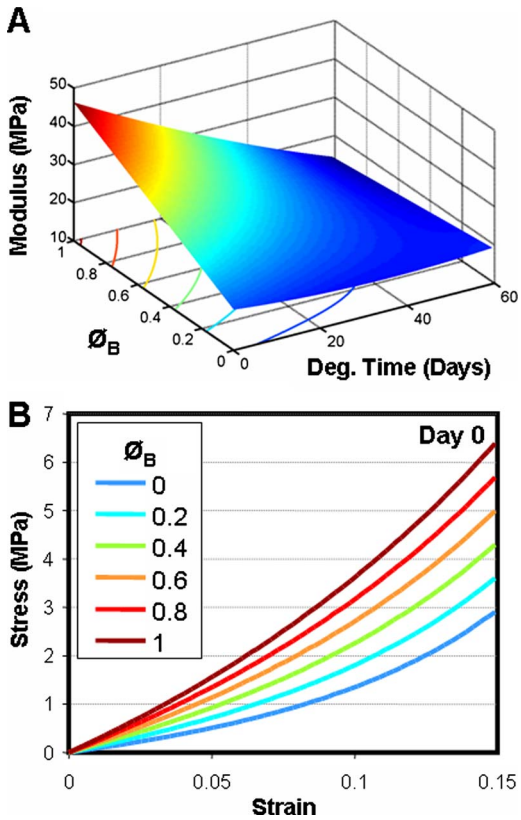

Fig. 6 Simulation of composite scaffolds of any formulation. (*a*) Behavior of composites covering the full range of possible PCL/blend combinations (as indicated by the initial mass fraction of blend fibers, $Ø^B$) was simulated for as-formed samples and with degradation over time. Modulus for each theoretical composite is denoted both by height as well as color. (*b*) Stress-strain behavior of composites of varying formulations on day 0.

specific mode of degradation of the blend fiber population and its influence on scaffold porosity will be important to characterize in future studies.

To better understand and predict the complex behaviors of nanofibrous scaffolds, which are further compounded when multiple-fiber populations are combined, a hyperelastic constitutive model was employed. The model fitted single-fiber population blend and PCL data well, despite the distinct stress-strain profiles of each. As evident from the experimental results, PCL was nonlinear along the fiber direction, while blend was mostly linear. The model reflected this, with a significant difference found between ξ^C and ξ^B. Without applying any constraints, fits to blend along the fiber direction invariably resulted in $\xi^B=0$, suggesting that the parameter values obtained were unique results of the curve fits, and thus the physical interpretations of these parameters were preserved. The model also described time-varying mechanics of the PCL and blend scaffolds, accounting for degradation through changes in the material parameters. Degradation of blend scaffolds was mirrored functionally by a significant decline in both the matrix (μ^B) and fiber (γ^B) terms. However, PCL, which demonstrated negligible mass loss and did not change in modulus, did not show changes in either μ^C or γ^C. The nonlinearity parameter, ξ^C, increased slightly with time.

We next validated the model by combining the constituent polymer parameters into a mixture model for the composite scaffold. Despite slightly underestimating stresses at the initial time point, the model provided very good approximations of the stress-strain behavior of composite scaffolds at all subsequent stages of degradation. The poor prediction at day 0 may suggest that, initially, the composite does not behave as a true mixture. This may be due to transient complex behaviors such as fiber-fiber welding or sliding, which diminish with degradation. Although homotypic fiber-fiber interactions are represented by the matrix phase, heterotypic fiber-fiber interactions, like those present in the composite, are not accounted for in the model. The experimental data may underscore this point, in that the fiber to transverse modulus ratio for PCL was 10:1, while for the blend it was only 3:1. It has previously been shown that small changes in solvent or environmental conditions can alter the degree of fiber-fiber welding that occurs with fiber deposition, changing tensile properties by as much as fourfold [44]. Nevertheless, the excellent prediction of composite behavior for days 7–63 of degradation demonstrates that the model not only fits curves, but that it represents a true description of static and time-varying mechanics of the composite material.

With the validated model, the complete range of possible blend and PCL combinations was simulated. This simulation demonstrated that the magnitude and time-dependence of composite scaffold mechanics can be modulated in a predictable fashion by altering the initial composition. Simulations also showed that it is possible to tune not only linear region modulus (Fig. 6(*a*)) but also the profile of the stress-strain curve. For instance, introducing an increasing fraction of PCL fibers to the composite reduces the modulus, while conferring nonlinearity to the overall material behavior. This model result is consistent with experimental observations of Studies I and II (Fig. 2(*d*)). Because many fiber-reinforced soft tissues are subjected to physiologic deformations below the transition strain, it is important to implement a method for scaffold design that incorporates full material nonlinearity and not only linear region metrics such as a single modulus value [6].

Taken together, this work represents a significant advance in the formulation of nanofibrous scaffolds for load-bearing applications and sets the stage for further advance. For example, it will be of great value to characterize the full elastic behavior of a wide collection of polymers. Model parameters from each would be integrated into a "functional library" that, coupled with the specific metrics taken from a tissue of interest, could be used to determine the exact composition and combination of fiber populations that would most closely reproduce the desired stress-strain profile. Such techniques can also define polymers that are not suitable for certain applications. For example, the polymer set employed here is not likely to be useful when rigorous load bearing is required at the time of implantation. The linear modulus of the composites generated in this study cannot exceed that of the stiffest element (26 MPa), a value far below that of many fiber-reinforced tissues. A stiffer, more slowly degrading element would be ideal as it could withstand physiologic loading and at the same time provide structural support to the construct, as other more rapidly eroding elements vacated the scaffold (in order to foster cell infiltration and matrix elaboration). We have recently made progress toward this goal with the electrospinning of select elements of a degradable poly(β-amino ester) library spanning a wide range of mechanical and degradation profiles [45], and new elastomeric and hydrolytically degradable polymers [46]. Combining these new polymers with rigorous mechanical testing and validated predictive models may result in improved scaffolds for implantation. This approach represents a novel direction in the rational design and fabrication of nanofibrous scaffolds for the repair or replacement of dense connective tissues.

Acknowledgment

This work was funded in part by the Aircast Foundation, a pilot grant from the Penn Center for Musculoskeletal Disorders (R.L.M., NIH Grant No. AR050950), the National Institutes of Health (R.L.M. and D.M.E., NIH Grant No. EB02425), and a Graduate Research Fellowship from the National Science Foundation (B.M.B.). The authors also gratefully acknowledge Ms. Giana Montero for her superb technical assistance.

References

[1] Lynch, H. A., Johannessen, W., Wu, J. P., Jawa, A., and Elliott, D. M., 2003, "Effect of Fiber Orientation and Strain Rate on the Nonlinear Uniaxial Tensile Material Properties of Tendon," ASME J. Biomech. Eng., **125**(5), pp. 726–31.

[2] Setton, L. A., Guilak, F., Hsu, E. W., and Vail, T. P., 1999, "Biomechanical Factors in Tissue Engineered Meniscal Repair," Clin. Orthop. Relat. Res., **Oct**(367), pp. S254–S272.

[3] Petersen, W., and Tillmann, B., 1998, "Collagenous Fibril Texture of the Human Knee Joint Menisci," Anat. Embryol. (Berl.), **197**(4), pp. 317–324.

[4] Petersen, W., Hohmann, G., Pufe, T., Tsokos, M., Zantop, T., Paulsen, F., and Tillmann, B., 2004, "Structure of the Human Tibialis Posterior Tendon," Arch. Orthop. Trauma Surg., **124**(4), pp. 237–242.

[5] Iatridis, J. C., MaClean, J. J., and Ryan, D. A., 2005, "Mechanical Damage to the Intervertebral Disc Annulus Fibrosus Subjected to Tensile Loading," J. Biomech., **38**(3), pp. 557–565.

[6] Butler, D. L., Shearn, J. T., Juncosa, N., Dressler, M. R., and Hunter, S. A., 2004, "Functional Tissue Engineering Parameters Toward Designing Repair and Replacement Strategies," Clin. Orthop. Relat. Res., **Oct**(427), pp. S190–S199.

[7] Awad, H. A., Butler, D. L., Harris, M. T., Ibrahim, R. E., Wu, Y., Young, R. G., Kadiyala, S., and Boivin, G., 2000, "In Vitro Characterization of Mesenchymal Stem Cell-Seeded Collagen Scaffolds for Tendon Repair: Effects of Initial Seeding Density on Contraction Kinetics," J. Biomed. Mater. Res., **51**(2), pp. 233–240.

[8] Costa, K. D., Lee, E. J., and Holmes, J. W., 2003, "Creating Alignment and Anisotropy Iin Engineered Heart Tissue: Role of Boundary Conditions in a Model Three-Dimensional Culture System," Tissue Eng., **9**(4), pp. 567–577.

[9] Thomopoulos, S., Fomovsky, G. M., and Holmes, J. W., 2005, "The Development of Structural and Mechanical Anisotropy in Fibroblast Populated Collagen Gels," ASME J. Biomech. Eng., **127**(5), pp. 742–750.

[10] Garvin, J., Qi, J., Maloney, M., and Banes, A. J., 2003, "Novel System for Engineering Bioartificial Tendons and Application of Mechanical Load," Tissue Eng., **9**(5), pp. 967–79.

[11] Moutos, F. T., Freed, L. E., and Guilak, F., 2007, "A Biomimetic Three-Dimensional Woven Composite Scaffold for Functional Tissue Engineering of Cartilage," Nature Mater., **6**(2), pp. 162–167.

[12] Cooper, J. A., Lu, H. H., Ko, F. K., Freeman, J. W., and Laurencin, C. T., 2005, "Fiber-Based Tissue-Engineered Scaffold for Ligament Replacement: Design Considerations and In Vitro Evaluation," Biomaterials, **26**(13), pp. 1523–1532.

[13] Altman, G. H., Horan, R. L., Lu, H. H., Moreau, J., Martin, I., Richmond, J. C., and Kaplan, D. L., 2002, "Silk Matrix for Tissue Engineered Anterior Cruciate Ligaments," Biomaterials, **23**(20), pp. 4131–4141.

[14] Reneker, D. H., and Chun, I., 1996, "Nanometre Diameter Fibres of Polymer, Produced by Electrospinning," Nanotechnology, **7**, pp. 216–223.

[15] Formhals, A., 1934, "Process and Apparatus for Preparing Artificial Threads," U.S. Patent No. 1,975,504.

[16] Burger, C., Hsiao, B. S., and Chu, B., 2006, "Nanofibrous Materials and Their Applications," Annu. Rev. Mater. Res., **36**, pp. 333–368.

[17] Li, W. J., Mauck, R. L., Cooper, J. A., Yuan, X., and Tuan, R. S., 2007, "Engineering Controllable Anisotropy in Electrospun Biodegradable Nanofibrous Scaffolds for Musculoskeletal Tissue Engineering," J. Biomech., **40**(8), pp. 1686–1693.
[18] Barnes, C. P., Sell, S. A., Boland, E. D., Simpson, D. G., and Bowlin, G. L., 2007, "Nanofiber Technology: Designing the Next Generation of Tissue Engineering Scaffolds," Adv. Drug Delivery Rev., **59**(14), pp. 1413–1433.
[19] Li, W. J., Mauck, R. L., and Tuan, R. S., 2005, "Electrospun Nanofibrous Scaffolds: Production, Characterization, and Applications for Tissue Engineering and Drug Delivery," J Biomed Nanotech, **1**(3), pp. 259–275.
[20] Stitzel, J., Liu, J., Lee, S. J., Komura, M., Berry, J., Soker, S., Lim, G., Van Dyke, M., Czerw, R., Yoo, J. J., and Atala, A., 2006, "Controlled Fabrication of a Biological Vascular Substitute," Biomaterials, **27**(7), pp. 1088–1094.
[21] Ding, B., Kimura, E., Sato, T., Fujita, S., and Shiratori, S., 2004, "Fabrication of Blend Biodegradable Nanofibrous Nonwoven Mats Via Multi-Jet Electrospinning," Polymer, **45**(6), pp. 1895–1902.
[22] Kidoaki, S., Kwon, I. K., and Matsuda, T., 2005, "Mesoscopic Spatial Designs of Nano- and Microfiber Meshes for Tissue-Engineering Matrix and Scaffold Based on Newly Devised Multilayering and Mixing Electrospinning Techniques," Biomaterials, **26**(1), pp. 37–46.
[23] Baker, B. M., Gee, A. O., Metter, R. B., Nathan, A. S., Marklein, R. A., Burdick, J. A., and Mauck, R. L., 2008, "The Potential to Improve Cell Infiltration in Composite Fiber-Aligned Electrospun Scaffolds by the Selective Removal of Sacrificial Fibers," Biomaterials, **29**(15), pp. 2348–2358.
[24] Sundaray, B., Subramanian, V., Natarajan, T., Xiang, R., Chang, C., and Fann, W., 2004, "Electrospinning of Continuous Aligned Polymer Fibers," Appl. Phys. Lett., **84**(7), pp. 1222–1224.
[25] Ayres, C., Bowlin, G. L., Henderson, S. C., Taylor, L., Shultz, J., Alexander, J., Telemeco, T. A., and Simpson, D. G., 2006, "Modulation of Anisotropy in Electrospun Tissue-Engineering Scaffolds: Analysis of Fiber Alignment by the Fast Fourier Transform," Biomaterials, **27**(32), pp. 5524–5234.
[26] Courtney, T., Sacks, M. S., Stankus, J., Guan, J., and Wagner, W. R., 2006, "Design and Analysis of Tissue Engineering Scaffolds That Mimic Soft Tissue Mechanical Anisotropy," Biomaterials, **27**(19), pp. 3631–3638.
[27] Nerurkar, N. L., Elliott, D. M., and Mauck, R. L., 2007, "Mechanics of Oriented Electrospun Nanofibrous Scaffolds for Annulus Fibrosus Tissue Engineering," J. Orthop. Res., **25**(8), pp. 1018–1028.
[28] Baker, B. M., and Mauck, R. L., 2007, "The Effect of Nanofiber Alignment on the Maturation of Engineered Meniscus Constructs," Biomaterials, **28**(11), pp. 1967–1977.
[29] Mathew, G., Hong, J. P., Rhee, L. M., Leo, D. J., and Nah, C., 2006, "Preparation and Anisotropic Mechanical Behavior of Highly-Oriented Electrospun Poly(Butylene Terephthalate) Fibers," J. Appl. Polym. Sci., **101**(3), pp. 2017–2021.
[30] De Vita, R., Leo, D. J., Woo, K. D., and Nah, C., 2006, "A Constitutive Law for Poly(Butylene Terephthalate) Nanofibers Mats," J. Appl. Polym. Sci., **102**(6), pp. 5280–5283.
[31] Nerurkar, N. L., Mauck, R. L., and Elliott, D. M., 2008, "ISSLS Prize Winner: Integrating Theoretical and Experimental Methods for Functional Tissue Engineering of the Annulus Fibrosus," Spine, **33**(25), pp. 2691–2701.
[32] Spencer, A. J. M., 1972, *Deformations of Fibre-Reinforced Materials*, Oxford University Press, London.
[33] Holzapfel, G. A., 2000, *Nonlinear Solid Mechanics: A Continuum Approach for Engineering*, Wiley, Chichester, p. 455.
[34] Eberlein, R., Holzapfel, G. A., and Schulze-Bauer, C. A., 2001, "An Anisotropic Constitutive Model for Annulus Tissue and Enhanced Finite Element Analyses of Intact Lumbar Disc Bodies," Comput. Methods Biomech. Biomed. Eng., **4**, pp. 209–230.
[35] Ogden, R. W., 1997, *Non-Linear Elastic Deformations*, Dover, New York.
[36] Ateshian, G. A., 2007, "Anisotropy of Fibrous Tissues in Relation to the Distribution of Tensed and Buckled Fibers," ASME J. Biomech. Eng., **129**(2), pp. 240–249.
[37] Bland, J. M., and Altman, D. G., 1986, "Statistical Methods for Assessing Agreement Between Two Methods of Clinical Measurement," Lancet, **1**(8476), pp. 307–310.
[38] Li, W. J., Cooper, J. A., Jr., Mauck, R. L., and Tuan, R. S., 2006, "Fabrication and Characterization of Six Electrospun Poly(Alpha-Hydroxy Ester)-Based Fibrous Scaffolds for Tissue Engineering Applications," Acta Biomater., **2**(4), pp. 377–85.
[39] Moffat, K. L., Kwei, A. S., Spalazzi, J. P., Doty, S. B., Levine, W. N., and Lu, H. H., 2008, "Novel Nanofiber-Based Scaffold for Rotator Cuff Repair and Augmentation," Tissue Eng., **15**(1), pp. 115–126.
[40] Fung, Y. C., 1982, *Biomechanics: Mechanical Properties of Living Tissues*, Springer-Verlag, New York.
[41] Guerin, H. A., and Elliott, D. M., 2005, "The Role of Fiber-Matrix Interactions in a Nonlinear Fiber-Reinforced Strain Energy Model of Tendon," ASME J. Biomech. Eng., **127**(2), pp. 345–350.
[42] Guo, Z. Y., Peng, X. Q., and Moran, B., 2006, "A Composites-Based Hyperelastic Constitutive Model for Soft Tissue With Application to the Human Annulus Fibrosus," J. Mech. Phys. Solids, **54**(9), pp. 1952–71.
[43] Baker, B. M., Nathan, A. S., Huffman, G. R., and Mauck, R. L., 2008, "Tissue Engineering With Meniscus Cells Derived From Surgical Debris," Osteoarthritis Cartilage, **17**(3), pp. 336–345.
[44] Kidoaki, S., Kwon, I. K., and Matsuda, T., 2006, "Structural Features and Mechanical Properties of In Situ-Bonded Meshes of Segmented Polyurethane Electrospun From Mixed Solvents," J. Biomed. Mater. Res., Part B: Appl. Biomater., **76B**(1), pp. 219–229.
[45] Tan, A. R., Ifkovits, J. L., Baker, B. M., Brey, D. M., Mauck, R. L., and Burdick, J. A., 2008, "Electrospinning of Photocrosslinked and Degradable Fibrous Scaffolds," J. Biomed. Mater. Res. Part A, **87A**(4), pp. 1034–1043.
[46] Ifkovits, J. L., Padera, R. F., and Burdick, J. A., 2008, "Biodegradable and Radically Polymerized Elastomers With Enhanced Processing Capabilities," Biomed. Mater., **3**(3), p. 034104.